



Improvement of forecast skill for severe weather by merging radar-based extrapolation and storm-scale NWP corrected forecast

Gaili Wang^{a,b,*}, Wai-Kin Wong^{c,1}, Yang Hong^{d,e,2}, Liping Liu^{a,3}, Jili Dong^{f,4}, Ming Xue^{f,4}

^a State Key Laboratory of Severe Weather, Chinese Academy of Meteorological Science, 46 Zhongguancun South Street, Haidian District, Beijing 100081, China

^b Jiangsu Institute of Meteorological Science, 16 Kunlun Road, Nanjing, Jiangsu 210009, China

^c Hong Kong Observatory, 134A, Nathan Road, Kowloon 999077, Hong Kong, China

^d School of Civil Engineering and Environmental, University of Oklahoma, 120 David L. Boren Blvd., National Weather Center Rm. 4610, Norman, OK 73072, USA

^e Department of Hydraulic Engineering, Tsinghua University, Beijing, 100084, China

^f School of Meteorology, and Center for Analysis and Prediction of Storms, University of Oklahoma, 120 David L. Boren Blvd., National Weather Center Rm. 4610, Norman, OK 73072, USA

ARTICLE INFO

Article history:

Received 18 June 2014

Received in revised form 16 October 2014

Accepted 28 October 2014

Available online 6 November 2014

Keywords:

Radar-based extrapolation

NWP forecasts

Error correction

Optimal merging

Severe storms

ABSTRACT

The primary objective of this study is to improve the performance of deterministic high resolution rainfall forecasts caused by severe storms by merging an extrapolation radar-based scheme with a storm-scale Numerical Weather Prediction (NWP) model. Effectiveness of Multi-scale Tracking and Forecasting Radar Echoes (MTaRE) model was compared with that of a storm-scale NWP model named Advanced Regional Prediction System (ARPS) for forecasting a violent tornado event that developed over parts of western and much of central Oklahoma on May 24, 2011. Then the bias corrections were performed to improve the forecast accuracy of ARPS forecasts. Finally, the corrected ARPS forecast and radar-based extrapolation were optimally merged by using a hyperbolic tangent weight scheme. The comparison of forecast skill between MTARe and ARPS in high spatial resolution of $0.01^\circ \times 0.01^\circ$ and high temporal resolution of 5 min showed that MTARe outperformed ARPS in terms of index of agreement and mean absolute error (MAE). MTARe had a better Critical Success Index (CSI) for less than 20-min lead times and was comparable to ARPS for 20- to 50-min lead times, while ARPS had a better CSI for more than 50-min lead times. Bias correction significantly improved ARPS forecasts in terms of MAE and index of agreement, although the CSI of corrected ARPS forecasts was similar to that of the uncorrected ARPS forecasts. Moreover, optimally merging results using hyperbolic tangent weight scheme further improved the forecast accuracy and became more stable.

© 2014 Elsevier B.V. All rights reserved.

* Corresponding author at: State Key Laboratory of Severe Weather, Chinese Academy of Meteorological Science, Beijing, 46 Zhongguancun South Street, Haidian District, Beijing 100081, China. Tel.: +86 10 5899 3540.

E-mail addresses: wgl3111@cams.cma.gov.cn (G. Wang), wkwong@hko.gov.hk (W.-K. Wong), yanghong@ou.edu (Y. Hong), lpiliu@cams.cma.gov.cn (L. Liu), jili.Dong@noaa.gov (J. Dong), mxue@ou.edu (M. Xue).

¹ Tel.: +852 2926 8642.

² Tel.: +1 405 325 3644.

³ Tel.: +86 10 5899 3540.

⁴ Tel.: +1 405 325 3502.

1. Introduction

Deterministic forecasting with high spatial and temporal resolutions for the next few hours (nowcasting) plays an important role in severe rainfall prediction, meteorological disaster warnings, and the meteorological services of major sports events. Three primary nowcasting methods are used operationally.

The first group includes a number of techniques that rely on extrapolation of radar images, and is widely applied in

operational nowcasting systems such as the Auto-Nowcast System (ANC; Mueller et al., 2003) developed by the National Center Atmosphere Research and the McGill Algorithm for Precipitation Nowcasting by Lagrangian Extrapolation (MAPLE; Turner et al., 2004) used at McGill. Extrapolation techniques are divided into pixel-based and object-based approaches (Zahraei et al., 2012). The pixel-based technique extrapolates radar reflectivity observations using motion estimation from two consecutive radar images (Rinehart and Garvey, 1978; Li et al., 1995; Grecu and Krajewski, 2000; Germann and Zawadzki, 2002; Zahraei et al., 2012; Wang et al., 2013; Sokol et al., 2013). The object-based technique identifies 3D convective cells, tracks, and forecasts storm-related parameters assuming linear trends (Dixon and Wiener, 1993; Johnson et al., 1998; Hong et al., 2004; Vila et al., 2008; Zahraei et al., 2013).

The second group consists of storm-scale NWP models. Recently, the “spin-up” problem of NWP models was reduced significantly using the rapid-update-cycle (RUC) approach. The High-Resolution Rapid Refresh (HRRR; Zahraei et al., 2012) developed by the National Oceanic and Atmospheric Administration, and ARPS used at the Center for Analysis and Prediction of Storms (CAPS) are the outstanding representatives of the second group. The forecast accuracy at the first several hours has been improved significantly by assimilating various types of observation data (Macpherson, 2001; Weygandt et al., 2002; Benjamin et al., 2004; Caya et al., 2005; Tong and Xue, 2005; Sokol, 2007; Sokol and Pesice, 2012; Wong et al., 2009; Zahraei et al., 2012).

Predictive accuracy of radar-based extrapolation rapidly decreases within the first several hours of severe weather development, because the growth and decay of storms are not taken into account. Extrapolation of observations is most likely more accurate in the shorter terms (Austin et al., 1987; Golding, 1998; Lin et al., 2005; Wong et al., 2009; Zahraei et al., 2012), as shown in Fig. 1. On the other hand, some comparisons show that the NWP models outperform radar-based extrapolation methods over longer time scales as they dynamically resolve large-scale flow. However, they may not produce optimal predictions at the first short-term, because they are sensitive to the initial condition, spatial resolution, and assimilation data (Golding, 1998; Ganguly and Bras, 2003; Lin et al., 2005; Zahraei et al., 2012).

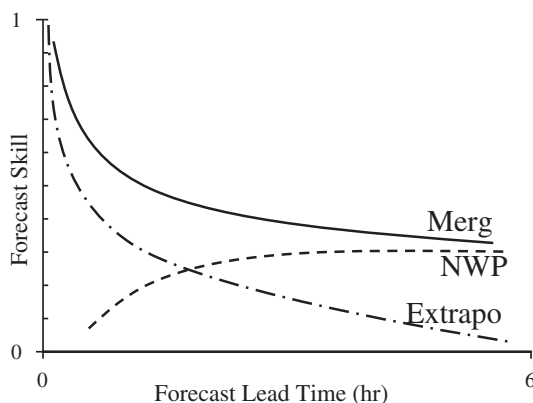


Fig. 1. Forecast performance of three primary nowcasting methods as a function of lead time (Wolfson et al., 2008).

Advantages of both approaches may be realized by a third group that merges or blends radar-based extrapolation with NWP-based forecast. The merging technique was primitively developed to advect rainfall fields using NWP model wind fields in the 1980s (Conway and Browning, 1988). A prior prototype of the forecasting approach is Nimrod system, which merges an extrapolation-based system, Forecasting Rain Optimised using New Techniques of Interactively Enhanced Radar and Satellite (FRONTIERS), with an NWP model referred to as Interactive Meso-scale Initialisation system using variational scheme and recursive filter algorithm (Golding, 1998). Recent nowcasting systems of the merging approach such as GANDOLF (Generating Advanced Nowcast for Deployment in Operational Land Surface Flood Forecast; Pierce et al., 2000), RAPIDS (Rainstorm Analysis and Prediction Integrated Data-processing System; Wong and Lai, 2006), and STEPS (Short-Term Ensemble Prediction System; Bowler et al., 2006) further validated the potential improvement upon the predictive skill, compared with individual forecast models. Optimal predictions could be obtained by assigning the primary weight to extrapolation forecasts for the first lead times, while the NWP forecasts are weighted to increase with lead time (Golding, 1998; Wong and Lai, 2006; Wong et al., 2009). The merged quantity was either rainfall rate (Golding, 1998; Pierce et al., 2000; Wong et al., 2009), radar reflectivity factor (Wilson and Xu, 2006), or a probabilistic forecast of precipitation (Bowler et al., 2006; Kober et al., 2012). Additionally, a bias-correction was applied for NWP model forecast before merging was performed (Wong et al., 2009). NWP models with coarse spatial resolution (≥ 10 km) and temporal resolution (1 h) were used, in most studies, to merge with radar-based extrapolation nowcast. A significant attempt to connect extrapolating nowcasting methods with numerical weather prediction models is the assimilation of extrapolated radar reflectivity data into a NWP model (Sokol, 2011).

Higher spatial and temporal resolution forecasts are needed to reduce casualties and property losses from rapidly changing severe weather events such as thunderstorms or flooding heavy rains. Radar networks were intended to provide very short-term (0–30 min) warning for high-impact severe weather events with rapid development and decay (Brewster, 2003). Predictive performance for these severe weather events could be improved by combining high spatial and temporal resolution storm-scale NWP with radar-based extrapolation.

This article aims to improve the performance of deterministic rainfall forecasts caused by the severe storms with high spatial and temporal resolutions by merging a radar-based extrapolation scheme with a storm-scale NWP model. A key element of this study is the use of the Advanced Regional Prediction System (ARPS) storm-scale NWP developed by the Center for Analysis and Prediction of Storms, University of Oklahoma. The ARPS model could output rainfall forecasts caused by severe storms with high spatial resolution of $0.01^\circ \times 0.01^\circ$ (~ 1 km \times 1 km) and 1-minute interval. Moreover, the deduced CPDF of radar observation for lead time is proposed for correcting the ARPS forecasts by using PDF matching. In this study, we evaluate the accuracy of forecasts using the Multi-scale Tracking and Forecasting Radar Echoes (MTaFRE) scheme, developed by the State Key Laboratory of Severe Weather (LaSW) of Chinese Academy of Meteorological Science (CAMS), versus the ARPS model for a violent tornado event that developed over parts of

western and much of central Oklahoma on 24 May, 2011. The performance of MTaRE model decreases rapidly with lead times because radar-based extrapolation ignores the temporal evolution of storms. The ARPS model could forecast the evolution of storms, but overestimates the storms.

The paper is organized as follows. Section 2 describes the study domain and data sets used in this study. The detailed methodology of bias-corrected ARPS forecasts and merging scheme is described in Section 3. Section 4 presents the evaluation results and discussion. The conclusions are drawn in Section 5.

2. Data and case study

2.1. Radar data

In this study, the radar mosaicked composite reflectivity factor product produced by the National Severe Storm Laboratory (NSSL) (Zhang et al., 2005) was used to track, nowcast future radar reflectivity factor fields, and also acts as verification data to assess forecast skill of MTaFRE and ARPS models. Radar mosaic composite reflectivity factor images were produced with a temporal resolution of 5 min and a spatial resolution of 0.01° (~ 1 km).

2.2. Case study and analysis domain

The May 21–26, 2011 tornado outbreak was used to experiment with the combination of MTaFRE forecasts and ARPS outputs. The tornado outbreak took place across the Midwestern and Southern regions of the United States and resulted in 184 deaths, making it the second deadliest since 1974, and the second costliest in United States history, with insured damage estimated at \$4–7 billion. Several tornadic thunderstorms developed over parts of western and much of central Oklahoma on May 24, 2011. Extensive damage occurred over many areas of central Oklahoma. Seven initialized times for predicting the tornado with up to 2 h lead times were analyzed in this paper.

3. Methodology

3.1. Performance indices

Performances of the radar-based extrapolation model, storm-scale NWP model, and bias-corrected scheme and merging forecast were qualitatively assessed using three performance indices. The index of agreement (d) was used to measure the agreement between forecasts and observations. The Critical Success Index (CSI) measures the pattern match between forecasts and observations. Germann and Zawadzki (2002) stated that neither the agreement nor the pattern match provided a direct measure of forecast accuracy. Thus, the mean absolute error (MAE) is calculated for measuring the average error magnitude. The formulas are defined as follows:

$$d = 1 - \frac{\sum_{i=1}^N (O_i - F_i)^2}{\sum_{i=1}^N (|O_i - \bar{O}| + |F_i - \bar{O}|)^2} \quad (1)$$

$$CSI = \frac{n_s}{n_s + n_f + n_a} \quad (2)$$

$$MAE = \frac{1}{N} \sum_{i=1}^N |F_i - O_i|, \quad (3)$$

where O_i and F_i are observed rainfall and predicted rainfall at the i th grid point, and the bar indicates the mean value. N is the number of observations and forecasts, while n_s , n_f , and n_a denote the number of successes, failures, and false alarms, respectively. When observed rainfall and predicted rainfall are equal, then a perfect forecast would result in $d = 1$, $CSI = 1$ and $MAE = 0$. The concepts of success, failure, false alarm are the same as those depicted in the literature (Grecu and Krajewski, 2000; Zahraei et al., 2012).

Although the forecasts were made in terms of radar reflectivity, we assessed them in terms of rainfall, which is not only a significant variable in hydrology but also a linear variable. Taking into account convective tornado storms, the single convective Z – R (where Z denotes radar reflectivity factor and R is rainfall rate) relationship was arbitrarily chosen as $Z = 300R^{1.4}$ for radar QPE, which was adopted operationally in the WSR-88D system. The rainfall estimate errors from the Z – R relationship are negligible because the effect on the forecasts is the same as that of observations and the errors from forecasts are likely to be much greater than those from estimates (Grecu and Krajewski, 2000). The threshold for calculating the CSI was selected to 0.1 mm h^{-1} . Precipitation rates below the threshold were considered as “no rain” (Germann and Zawadzki, 2004).

3.2. Multi-scale Tracking and Forecasting Radar Echoes (MTaFRE) scheme

MTaFRE is an extrapolation-based nowcasting technique for deterministic forecasts (see detail description in Wang et al., 2013, 2014). A flowchart of the MTaFRE scheme is given in Fig. 2. It uses a two-step Tracking Radar Echoes by Cross-correlation (TREC) algorithm to estimate motion of a storm, and a mass-conserving, monotonic advection scheme based on the explicit remapped particle-mesh semi-Lagrangian (RPMSL) advection scheme for extrapolating reflectivity factor fields (Reich, 2007). The length step was chosen to be 5 min, corresponding to the temporal resolution of radar observations. For improving forecasting accuracy, moving average as a function of lead time is adopted to filter off the perishable and less predictable small-scale precipitation features. The optimal smoothing window length is given as follows:

$$L = kT^\lambda, \quad (4)$$

where L is a moving average window in km, T denotes lead time in min, k and λ are empirical coefficients with ranges of $1.0 \leq k \leq 1.3$ and $0.7 \leq \lambda \leq 0.8$, respectively. The relationship depends on the assessment parameter and is independent of precipitation classification (Bellon and Zawadzki, 1994; Seed, 2003). Because of the RPMSL advection scheme outputting forecasts in 5-min interval, a spatially moving average centered on each pixel and including a matrix in size of (3×3) pixels ($\sim 3 \text{ km} \times 3 \text{ km}$) is applied to each forecast pattern.

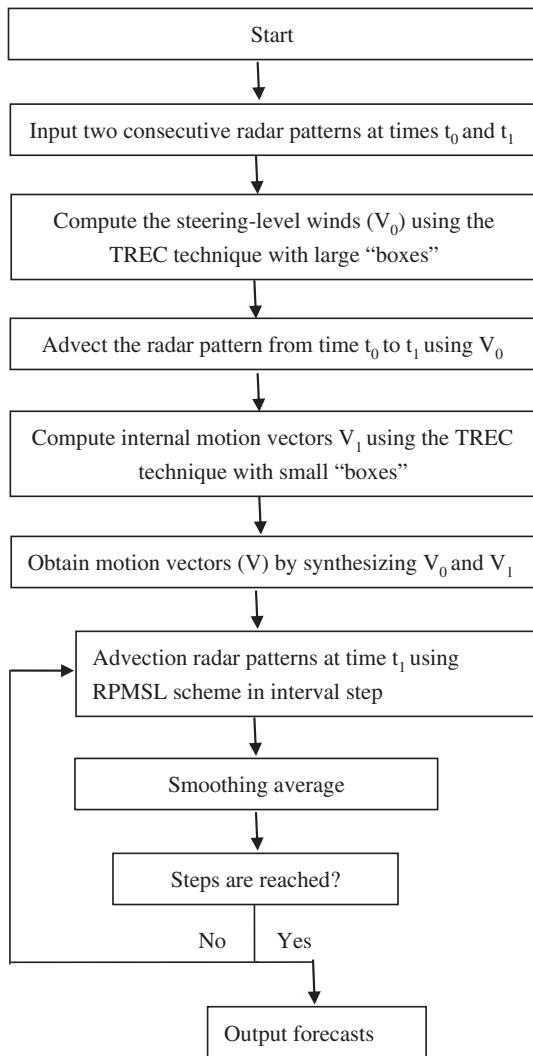


Fig. 2. A flowchart of the MTaFRE scheme.

The MTaFRE ran the NSSL composite reflectivity factor images to generate up to 2-h forecasts with a horizontal resolution of $0.01^\circ \times 0.01^\circ$ and a temporal resolution of 5 min.

3.3. Advanced Regional Prediction System (ARPS)

The Advanced Regional Prediction System (ARPS) is a state-of-the-art storm-scale forecasting model (Xue et al., 2000, 2001, 2003), which was used as the storm-scale NWP model in this study. ARPS is a compressible non-hydrostatic model that predicts velocity components u , v , and w , potential temperature θ , pressure p , turbulence kinetic energy (TKE), water vapor mixing ratio q_v , and the mixing ratios of cloud water, rainwater, ice, snow, and hail (q_c , q_r , q_i , q_s , and q_h , respectively). A $353 \times 323 \times 53$ grid with a horizontal resolution of 1 km defines the whole physical domain of a $350 \times 320 \times 20$ km³ area. In the vertical, a grid stretching scheme based on a cubic function is used with the mean vertical grid spacing of 400 m and a grid spacing of 20 m at the surface. The 3-ice microphysical scheme is used (Lin et al., 1983). Subgrid-scale

turbulence mixing is handled by the 1.5-order TKE-based turbulence parameterization after Deardorff (1980), while within the convective planetary boundary layer (PBL) a non-local vertical mixing length is calculated based on Sun and Chang (1986).

Other model dynamics choices include fourth-order momentum advection used in both the horizontal and vertical. A fourth-order monotonic flux-corrected transport (FCT) scheme (Zalesak, 1979) is applied to potential temperature, water variables, and TKE. Details on these physics and computational options can be found in Xue et al. (2000, 2001, 2003).

To initialize the forecasts, the North American Meso-scale Model (NAM; Janjic, 2003) 12-km analysis is first interpolated to the ARPS high-resolution domain. The radar observations, including radar radial velocity and reflectivity factor, are assimilated with a three-dimensional variational (3D-Var) cloud analysis system (Gao et al., 2004; Brewster, 2003; Hu et al., 2006a, b) within the Advanced Regional Prediction System to obtain the initial conditions.

The intense degree of high-impact severe weather events is usually expressed in terms of reflectivity factor. Radar reflectivity factor is calculated from ARPS forecast based on Smith et al. (1975), which is not an ARPS forecast variable. The logarithmic reflectivity factor Z in dBZ is estimated as follows:

$$Z = 10 \log_{10} \left(\frac{Z_e}{1 \text{mm}^6 \text{m}^{-3}} \right), \quad (5)$$

where, the reflectivity factor (Z_e) is composed of three contributions from rainwater, snow, and hail. This formula has been used by Tong and Xue (2005).

ARPS was initialized every 20-min from 2100 to 2300 UTC on May 24, 2012 to forecast the evolution of the tornado up to 2-h ahead, with high spatial resolution of $0.01^\circ \times 0.01^\circ$ and forecast output interval of 1 min. The ARPS forecasts of a 5-min interval were chosen to be evaluated and merged with radar observations. The ARPS outputs for the tornado event focused on the domain from 95.5 W to 99.5 W in longitude and from 33.5 N to 36.1 N in latitude.

3.4. Bias correction for ARPS forecasts

Storm-scale forecast fields may have properly developed small-scale features that have incorrect positions or improper amplitudes (Hoffman et al., 1995). Analysis and correction of position error and amplification error could also improve the forecast by reducing the differences between the analysis fields and observations (Hoffman and Grassotti, 1996; Brewster, 2003). Taking into account the ARPS model forecasting correct positions for the tornado event, an amplitude-correcting scheme was adopted to improve forecast accuracy of the ARPS model in this study.

Due to physical processes, initial condition and model resolution, intensity discrepancies between NWP forecasts and the observations are notable (Wong et al., 2009). In this work, the amplitude correction is performed for the ARPS forecasts by matching the Probability Density Function (PDF) of the ARPS forecast field with that of the radar observation field. Cumulative PDF (CPDF), defined as the PDF for reflectivity factor equal to or larger than a threshold, is then computed for the ARPS forecast field and the radar observation field,

respectively. Assuming that reflectivity factor at a percentage point in the CPDF table for ARPS forecast field is the same as that in the CPDF table for the observation field, the bias of amplitude in the ARPS forecast is corrected by matching the CPDF of the ARPS forecast field with that of the radar observation field. The PDF matching scheme was used to calibrate 1-h accumulated precipitation forecasts of the Non-hydrostatic Model (NHM) by matching PDF of precipitation intensity of NHM with that of quantitative precipitation estimation from radar. Then, when no radar observations were available for matching with NHM forecast at subsequent lead time, precipitation intensity of NHM at the lead time was corrected by using the ratio of its maximum precipitation value to that at calibrating time (Wong et al., 2009). It seems unstable that amplification correction typically depends on a single value of maximum. Xie and Xiong (2011) adopted a PDF matching method in correcting daily precipitation estimation produced by the Climate Prediction Center morphing method (CMORPH). In this study, we extended the work to deduce PDFs of observations at lead times when no actual radar observations were available, and corrected the amplitude errors of ARPS forecasts by using PDF matching.

Major steps of the ARPS model amplitude correcting scheme are outlined with the following three steps:

- (i) Calculate the PDF of ARPS forecasts and MTaFRE forecasts at 5-min lead time;

Previous studies have shown that the Weibull distribution is reasonable for fitting precipitation, and provides better fit than the gamma distribution for many meteorological applications (Wong, 1977; Shoji and Kitaura, 2006; Wong and Lai, 2006). In this paper, the Weibull distribution with two shape parameters was used to fit intensity of storms. The PDF and CPDF of Weibull distribution are expressed using Eqs. (6) and (7), respectively:

$$f(x) = \frac{k}{\lambda} \left(\frac{x}{\lambda}\right)^{k-1} e^{-\left(x/\lambda\right)^k}, \tag{6}$$

$$F(x) = P\{t < x\} = \int_{-\infty}^x f(t) dt = 1 - e^{-\left(x/\lambda\right)^k}, \tag{7}$$

where $k > 0$ is the shape parameter and $\lambda > 0$ is the scale parameter of the Weibull distribution. Studies have shown that Maximum likelihood method is simple and has higher fitting precision for estimating Weibull distribution parameters (Zhang, 1996; Ghosh, 1999). Therefore, in this study, the maximum-likelihood estimator method was used to estimate Weibull distribution parameters.

- (ii) Amplitude error correction was performed for ARPS forecasts at 5-min lead time using PDF matching and improvement of forecast accuracy was evaluated;

When no radar observation was available at the lead time and radar-based extrapolation was effective for forecasting at the 5-min lead time, the +5 minute MTaFRE prediction was regarded as equal to radar observation. Therefore, amplitude error correction is first performed for the +5 minute ARPS prediction by PDF matching. Both CPDFs of the ARPS forecast field and MTaFRE forecast field at the 5-min lead time are

computed, respectively. We assume that reflectivity factor at a percentage point in the CPDF table for the +5 minute ARPS prediction is the same as that in the CPDF table for the +5 minute MTaFRE prediction. The amplitude error correction for ARPS forecasts at the 5-min lead time is performed by matching its CPDF with that of the simultaneous MTaFRE forecasts. For example, if the 70 percentile values in the CPDF table for ARPS forecast field and MTaFRE forecast field are 50 dBZ and 45 dBZ, respectively, reflectivity factor of 50 dBZ in ARPS forecast field will be adjusted to 45 dBZ so that the CPDF of the corrected ARPS forecast field will be the same as that for the MTaFRE forecast field. Then the MAEs are compared (before and after correction) to determine whether the correction procedure could be performed for the ARPS forecast fields at subsequent lead times.

- (iii) If step (ii) improved the forecast accuracy, deduce PDFs of radar observations (named deduced PDF) at subsequent lead times, then PDF matching was adopted for correcting ARPS forecasts at subsequent lead times.

With increasing lead time, the difference between MTaFRE prediction and radar observation increases gradually. It is not reasonable to correct the ARPS prediction by using the MTaFRE prediction. Therefore, in this study, we deduced CPDFs of radar observations for subsequent lead times when no radar observations were available. For example, for the tornado event at 2140 UTC 24 May 2011, assuming that we intended to deduce the CPDF for +50 minute radar observation, we first computed CPDF for +5 minute MTaFRE prediction, and CPDFs for +5 and +50 minute ARPS predictions, respectively. Then two hypotheses were made: (1) +5 minute MTaFRE prediction is regarded as +5 minute radar observation; and (2) Evolution of the storm predicted by the ARPS model is consistent with that of radar observations in the same period. That is, the change of reflectivity factor at a percentage point between CPDF tables for +5 and +50 minute ARPS predictions is regarded as the same as that for radar observations. Fig. 3 gives an example, the 70 percentile values in the CPDF tables for +5 and +50 minute ARPS predictions are 32 dBZ and 42 dBZ, respectively. The 70 percentile values in the CPDF table for +50 minute ARPS prediction increased by Δ dBZ (10 dBZ), compared to that for +5 minute ARPS prediction. The 70 percentile values in the CPDF table for +5 minute MTaFRE prediction (regarded as radar observation) are 25 dBZ.

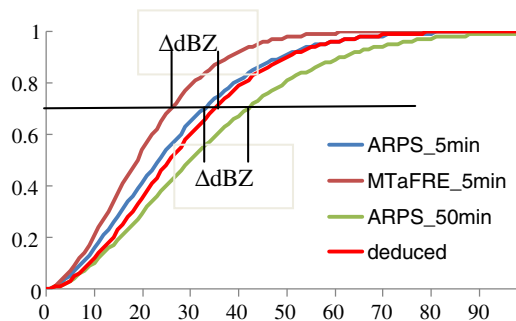


Fig. 3. Schematic diagram of deduced CPDF of observation corresponding to ARPS forecast field at 50-min lead time initialized at 2140 UTC 24 May 2011.

Based on the above two hypotheses, we obtain that the 70 percentile values in the CPDF table for +50 minute radar observation also have an equal increment of ΔdBZ (10 dBZ). Thus, we deduce that the 70 percentile values in the CPDF table for +50 minute radar observation should be 35 dBZ. Therefore, reflectivity factor of 42 dBZ in the +50 minute ARPS prediction will be adjusted to 35 dBZ. Repeating the procedure, the deduced CPDF of the +50 minute radar observation is obtained (red solid line in Fig. 3), and the +50 minute ARPS prediction will be corrected.

3.5. Merging scheme

MTaRE with ARPS was merged by implementing a weighted average of the single forecast product. Studies have verified that radar-based extrapolation forecasts outperform numerical weather prediction models at short lead times. However, the NWP models perform better than extrapolation methods with increasing lead times (Lin et al., 2005). Therefore, in the merging scheme, larger weights are usually assigned to extrapolation forecasts at very short lead times and increasing weights are given to NWP models with lead time increasing (Wong et al., 2009). The merging forecasts are obtained using Eq. (8):

$$R_{\text{merging}}(t) = (1-w(t)) \times R_{\text{extra}}(t) + w(t) \times R_{\text{NWP}}(t), \quad (8)$$

where $R_{\text{merging}}(t)$ is the merging forecast at a lead time (t) , $R_{\text{extra}}(t)$, and $R_{\text{NWP}}(t)$ are extrapolation forecast and NWP forecast, respectively, at lead time (t) , and $w(t)$ is the weight of the NWP model forecast. Yang et al. (2010) compared three weight schemes among sine curve weight, hyperbolic tangent curve weight, and real-time scrolling weight, and showed that the merging results with hyperbolic tangent curve weight were closer to observations. The weight calculated by the hyperbolic tangent curve can be expressed using Eq. (9):

$$w(t) = \alpha + \left(\frac{\beta - \alpha}{2} \right) \times \{1 + \tanh[\gamma(t-1)]\}, \quad (9)$$

where α and β are the weights at lead times of $t = 0$ and $t = 1$ h, respectively. They can be determined from evaluation results of past forecasts. In this study, α was set to 0.2 and β was set to 0.7 according to past forecasts, and γ represents the slope of the middle section of the hyperbolic tangent curve. To make $w(t)$ smoother in the middle section of the hyperbolic tangent curve, γ is set to 1. Based on the above, the merging forecasts are mainly based on radar-based extrapolation at lead times in the first half hour, and the weight of the NWP model increases gradually with increasing lead times.

4. Results and discussion

4.1. Comparison of performance between MTaFRE and ARPS forecasts

The forecast performances of MTaFRE and ARPS were compared for up to 2-h forecasts initiated at 7 times of 2100, 2120, 2140, 2200, 2220, 2240, and 2300 UTC 24 May 2012. The aim of the evaluation was to compare the advantages and disadvantages of MTaFRE and ARPS models.

Fig. 4 shows an example of comparison of forecast fields from MTaFRE and ARPS models initialized at 2140 UTC 11 May 2011 with radar observations. Fig. 5 gives the mean forecast performances for all the lead times from 5 min to 2 h over the 7 initialized times using three performance indices. MTaFRE forecasts quite well during the first 30-min lead times; however, MTaFRE could not forecast the evolution of the violent storm with increasing lead time. The MTaFRE model has a higher initial CSI (0.92) than ARPS (0.73) at the 5-min lead time; however, the forecast accuracy decreases with increasing lead time and is worse than the ARPS model after a lead time of 50 min. The loss of accuracy for the MTaFRE radar-based extrapolation is due to temporal evolution of storms. On the other hand, ARPS could forecast the enhancement of a violent tornado, which complements the shortcomings of radar-based extrapolation, but ARPS forecast significantly overestimates storm intensity of the tornado event. This results in MAE of ARPS being much higher than that of MTaFRE for all the lead times from 5 min to 2 h. The index of agreement for MTaFRE is slightly better than ARPS for all the lead times.

4.2. Error correction for ARPS forecast fields

The original ARPS forecast fields exhibited much higher values of reflectivity factor compared to radar observations, which was effectively improved by the PDF matching scheme. Fig. 6 gives the amplitude-corrected ARPS forecasts initialized at 2140 UTC 11 May 2011, which shows that the amplitude correction procedure successfully reduced the errors of original ARPS forecasts and produced a more accurate reflectivity factor field.

Effectiveness of the amplitude correction procedures was qualitatively evaluated for improved forecast accuracy by comparing the index of agreement, CSI, and MAE for original and corrected ARPS forecast fields at the available 7 initialized times. Fig. 7 shows the comparison of the performances between original and corrected ARPS forecast fields up to the lead time of 2 h with 10-min interval initialized at 2140 UTC 11 May, 2011. The corrected ARPS forecast fields have a higher index of agreement and substantially reduced MAE for all the lead times, compared with original ARPS forecast. Corrected ARPS forecast fields have no significant improvement on CSI. At some lead times, corrected ARPS forecast fields have lower CSI than the original ARPS forecast fields. This may be due to amplitude correction error that perished CSI by adjusting some original values less than the evaluation threshold.

From the mean performance indexes of the corrected ARPS forecasts over 7 initialized times (Fig. 5), the amplitude correction scheme is shown to improve the index of agreement of the ARPS forecast fields, and is comparable to that of the MTaRE model. The corrected ARPS forecast fields have significantly reduced the MAE compared with their original forecast fields, although its MAE is still slightly higher than MTaREs. However, the correction scheme has negligible improvement in terms of CSI.

During amplitude correction, the first assumption is that MTaFRE forecast field at the lead time of 5 min is the same as a radar observation. Studies showed negligible error between the radar-based extrapolation of 5-min lead time and radar observation. The second assumption is that the ARPS model forecasts a storm's evolution consistent with radar observations,

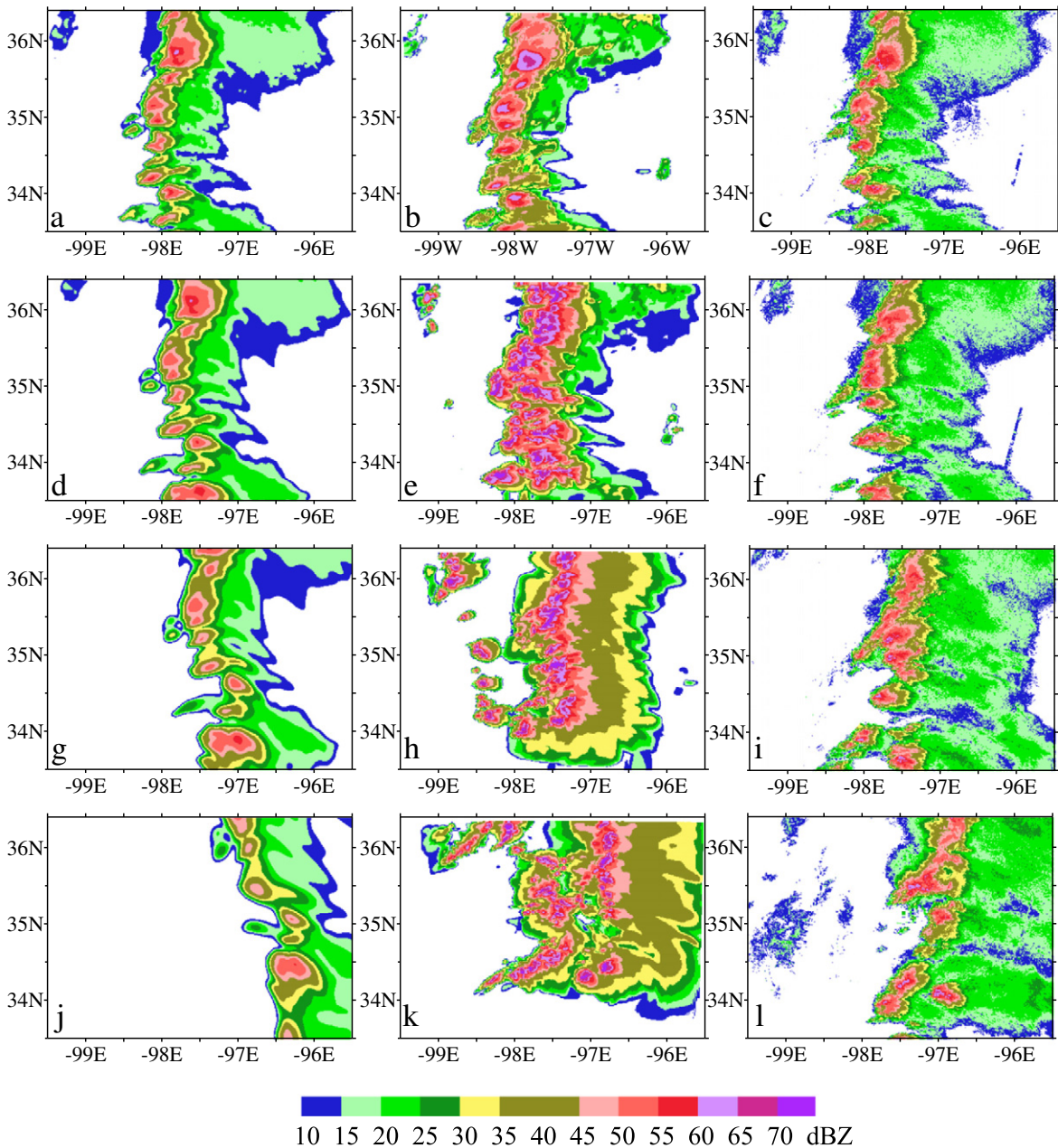


Fig. 4. Comparison of forecast fields from ARPS and MTaFRE models initialized at 2140 UTC 11 May 2011 with radar observations, a, b, d, e, g, h, and j (k) represent MTaFRE (ARPS) forecast fields at the lead times of 10 min, 30 min, 60 min, and 90 min; c, f, i and l are corresponding radar observations.

so the error depends on the performance of the NWP model. In general, we can see that the MAE of ARPS forecast was significantly reduced and index of agreement was improved.

4.3. Merging results

Very-short term forecasts from radar-based extrapolation and storm-scale NWP have their respective advantages and disadvantages. Although the ARPS forecasts have been corrected, MTaFRE models have better CSI during the first 20 min lead times, and better index of agreement and MAE for all lead times.

After a lead time of 50 min, both original and bias-corrected ARPS forecasts have better CSI than the MTaFRE model. Studies have shown that merging different forecast members could produce a better and stable forecast (Raftery et al., 2005; Ajami et al., 2007; Slougheter et al., 2007; Jiang et al., 2012). In this study, two different deterministic forecast fields with high spatio-temporal resolution were merged and evaluated.

Fig. 8 gives the merging forecasts of MTaFRE and ARPS forecasts initialized at 2140 UTC 11 May 2011. Compared with radar observations (Fig. 4f and i), it can be seen that the merging forecasts not only could predict the temporal evolution

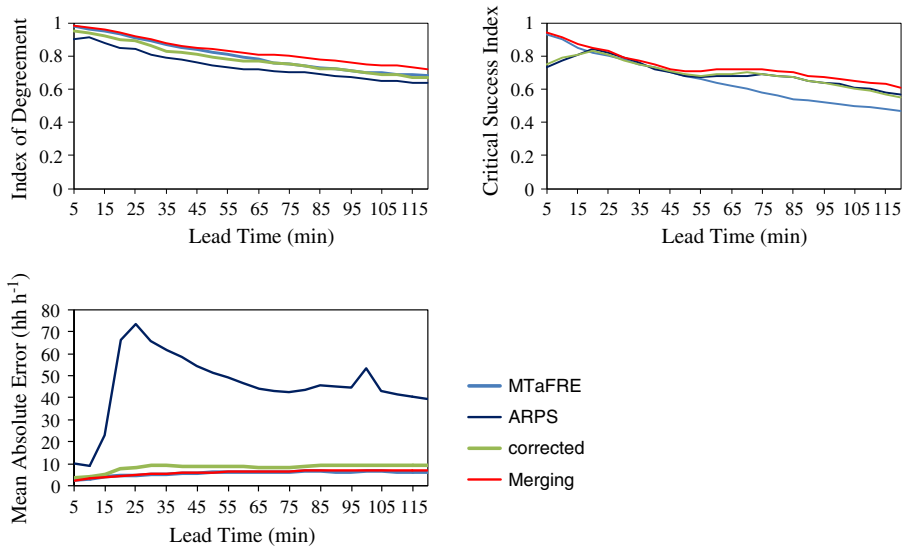


Fig. 5. Mean forecast accuracy of MTaFRE, ARPS, bias-corrected ARPS, and merging forecasts up to the lead time of 2 h over 7 initialized times.

of the tornado, but also were close to radar observations in terms of intensity. Quantitative evaluation also demonstrated the improvement of forecast performances. Fig. 9 represents the calculated performance indexes at 60-min lead time for 7 initialized times, and shows that the merging forecasts have better index of agreement and CSI compared with each individual forecast (except for the initialized time of 2300 UTC). They also have MAE that is comparable to radar-based extrapolation.

From the mean forecast performances over the 7 initialized times (Fig. 5), the merging results are better than or similar to the best of the forecasts from the single forecast product. The results show that the merging forecasts significantly improved the forecast performances of all the lead times in this study to a better and more stable direction in terms of both index of agreement and CSI, though there was no significant improvement as far as MAE relative to the MTaRE model is concerned. Note that the forecast accuracy of the merging forecasts depends on that of each single model.

5. Conclusions

Radar-based extrapolation and storm-scale NWP models are two major very short-term deterministic forecast methods. In this study, the forecast accuracy of MTaRE model developed by the State Key Laboratory of Severe Weather of Chinese Academy of Meteorological Science was compared with the ARPS model developed by the Center for Analysis and Prediction of Storms, University of Oklahoma. Amplitude error corrections were then performed on the ARPS forecasts using PDF matching. Finally, the corrected ARPS forecasts and MTaRE forecasts were merged using hyperbolic tangent curve weight scheme.

Results show that both radar-based extrapolation and storm-scale NWP model have individual advantages and limitations. The MTaRE model was able to predict the existing storms, but could not forecast the temporal evolution. The ARPS model did not have this limitation, but the ARPS overestimated the storm intensity. The MTaRE model outperforms the ARPS model as far as index of agreement and MAE are concerned. The MTaRE has

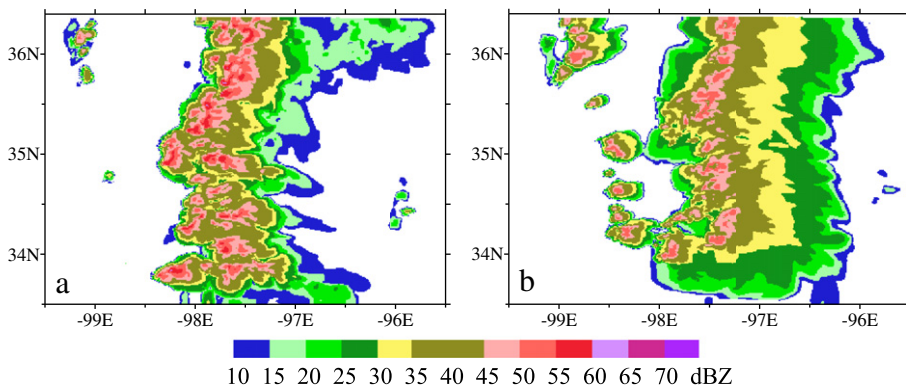


Fig. 6. Amplitude-corrected ARPS forecasts initialized at 2140 UTC 11 May 2011. 30 min lead time (a) and 60 min lead time (b).

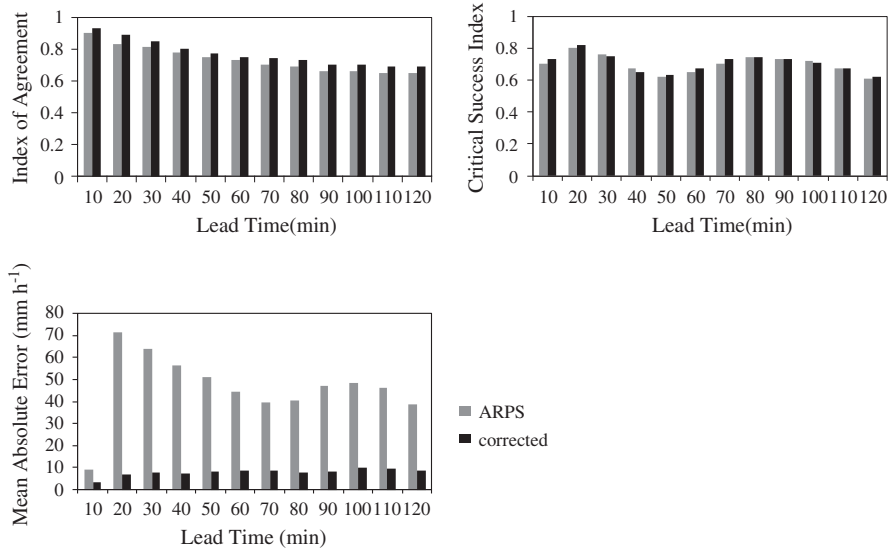


Fig. 7. Corrected ARPS forecast fields with original ARPS forecast fields initialized at 2140 UTC 11 May 2011.

better CSI than the ARPS model during the first 20-min lead times and comparable CSI to the ARPS model for lead times ranging from 20 min to 50 min, while after 50 min lead times the ARPS model has better CSI than MTaRE.

The amplitude error correction scheme improves ARPS forecasts in terms of MAE and index of agreement, although it has no significant improvement on CSI relative to original ARPS forecasts. In short, the amplitude error correction approach demonstrated a positive effect for forecast performance of the ARPS model.

Forecasts of the MTaRE and the corrected ARPS were merged using hyperbolic tangent curve weight scheme, which achieved the best index of agreement and CSI for all initialized times modeled for the Oklahoma tornado event in May 2011. Still, the merging forecasts also further reduced MAE of the corrected ARPS forecasts and resulted in a similar MAE to the MTaRE model. Overall, the merging results are better than or similar to the best of the forecasts from the single forecast product. The merging method significantly improved the forecast

performance of all the lead times from 5 min to 2 h. This study also confirms that merging radar-based extrapolation with storm-scale NWP is one of the primary means to improve the short-term deterministic rainfall forecasts caused by severe storms. The performance of merging forecast scheme is closely related with that of each single forecast member. Therefore, it is a key step to improving the forecast accuracy of each single forecast member.

This merging scheme was assessed quantitatively based on just a tornado event and 24 forecasts and should be considered to be preliminary. Further investigations should focus on error correction of storm-scale NWP model and the merging approach using more events. Currently, a WRF-based rapid updating cycling forecast system of Beijing Meteorological Bureau (BJ-RUC) is one of major storm-scale NWP in China. Several heavy convective precipitation events that occurred in Beijing are being selected for investigating the merging technique based on BJ-RUC and MTaRE. Larger amounts of data will be used to evaluate the merging scheme.

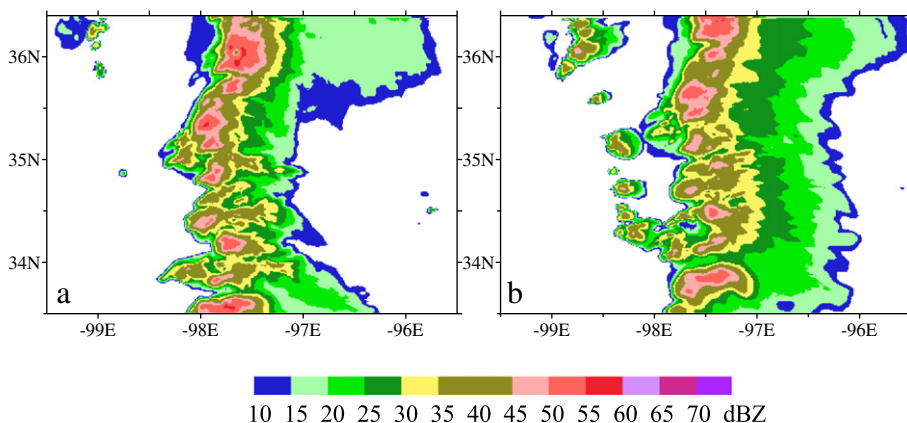


Fig. 8. Merging forecasts of MTaFRE and ARPS initialized at 2140 UTC 11 May 2011 with 30-min lead time (a) and 60-min lead time (b).

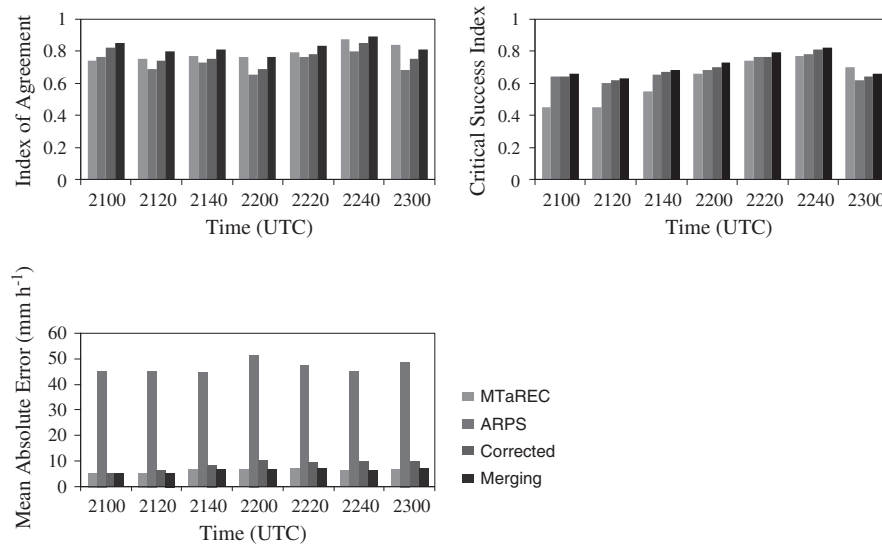


Fig. 9. Comparison of forecast performances among MTaFRE, ARPS, corrected ARPS, and merging forecasts at the lead time of 60 min for 7 initialized times.

Acknowledgments

This study was supported by the Special Fund for Basic Research and Operation of Chinese Academy of Meteorological Science (Grant No. 2011Y004) and Beijing fund of Jiangsu Institute of Meteorological Science (Grant No. BJG201303). The authors would also acknowledge the HyDROS lab (<http://hydro.ou.edu>) at the National Weather Center Advanced Radar Research Center (<http://arrc.ou.edu>) and Hong Kong Observatory for providing academic exchanges and visits.

References

- Ajami, N.K., Duan, Q.Y., Sorooshian, S., 2007. An integrated hydrological Bayesian multimodel combination framework: confronting input, parameter, and model structural uncertainty in hydrologic prediction. *Water Resour. Res.* 43, W01403.
- Austin, G.L., Bellon, A., Dionne, P., Roch, M., 1987. 1987: on the interaction between radar and satellite image nowcasting systems and mesoscale numerical models. *Proceedings, Symposium on Mesoscale Analysis and Forecasting, Vancouver, ESA SP-282*, pp. 225–228.
- Bellon, A., Zawadzki, I., 1994. Forecasting of hourly accumulations of precipitation by optimal extrapolation of radar maps. *J. Hydrol.* 157, 211–233.
- Benjamin, S.G., Devenyi, D., Weygandt, S.S., Brundage, K.J., Brown, J.M., Grell, G.A., Kim, D., Schwartz, B.E., Smirnova, T.G., Smith, T.L., Manikin, G.S., 2004. An hourly assimilation-forecast cycle: the RUC. *Mon. Weather Rev.* 132, 495–518.
- Bowler, N., Pierce, C., Seed, A., 2006. STEPS: a probabilistic precipitation forecasting scheme which merges an extrapolation nowcast with down-scaled NWP. *Q. J. R. Meteorol. Soc.* 132, 2127–2155.
- Brewster, K.A., 2003. Phase-correcting data assimilation and application to storm-scale numerical weather prediction. Part I: method description and simulation testing. *Mon. Weather Rev.* 131, 480–492.
- Caya, A., Sun, J., Snyder, C., 2005. A comparison between 4DVAR and the ensemble Kalman filter technique for radar data assimilation. *Mon. Weather Rev.* 133, 3081–3093.
- Conway, B.J., Browning, K.A., 1988. Weather forecasting by interactive analysis of radar and satellite imagery. *Phil. Trans. R. Soc. London A324*, 299–315.
- Deardorff, J.W., 1980. Stratocumulus-capped mixed layers derived from a three-dimensional model. *Bound.-Layer Meteorol.* 18 (4), 495–527.
- Dixon, M., Wiener, G., 1993. TITAN: thunderstorm identification, tracking, analysis and nowcasting—a radar-based methodology. *J. Atmos. Ocean. Technol.* 10, 785–797.
- Ganguly, A.R., Bras, R.L., 2003. Distributed quantitative precipitation forecasting using information from radar and Numerical Weather Prediction models. *J. Hydrometeorol.* 4 (6), 1168–1180.
- Gao, J., Xue, M., Brewster, K., Droegemeier, K.K., 2004. A three-dimensional variational data analysis method with recursive filter for Doppler radars. *J. Atmos. Ocean. Technol.* 21, 457–469.
- Germann, U., Zawadzki, I., 2002. Scale-dependence of the predictability of precipitation from continental radar images. Part I: description of the methodology. *Mon. Weather Rev.* 130 (12), 2859–2873.
- Germann, U., Zawadzki, I., 2004. Scale-dependence of the predictability of precipitation from continental radar images. Part II: probability forecasts. *J. Appl. Meteorol.* 43, 74–89.
- Ghosh, A., 1999. A FORTRAN program for fitting Weibull distribution and generating samples. *Comput. Geosci.* 25, 729–738.
- Golding, B.W., 1998. Nimrod: a system for generating automated very short range forecasts. *Meteorol. Appl.* 5 (1), 1–16.
- Greco, M., Krajewski, W.F., 2000. A large-sample investigation of statistical procedures for radar-based short-term quantitative precipitation forecasting. *J. Hydrol.* 239, 69–84.
- Hoffman, R.N., Grassotti, C., 1996. A technique for assimilating SSM/I observations of marine atmospheric storms with ECMWF analyses. *J. Appl. Meteorol.* 35, 1177–1188.
- Hoffman, R.N., Liu, Z., Louis, J.F., Grassotti, C., 1995. Distortion representation of forecast errors. *Mon. Weather Rev.* 123, 2758–2770.
- Hong, Y., Hsu, K., Sorooshian, S., Gao, X., 2004. Precipitation estimation from remotely sensed imagery using an Artificial Neural Network cloud classification system. *J. Appl. Meteorol.* 43, 1834–1853.
- Hu, M., Xue, M., Brewster, K., 2006a. 3DVAR and cloud analysis with WSR-88D level-II data for the prediction of Fort Worth tornadic thunderstorms. Part I: cloud analysis and its impact. *Mon. Weather Rev.* 134, 675–698.
- Hu, M., Xue, M., Gao, J., Brewster, K., 2006b. 3DVAR and cloud analysis with WSR-88D level-II data for the prediction of Fort Worth tornadic thunderstorms. Part II: impact of radial velocity analysis via 3DVAR. *Mon. Weather Rev.* 134, 699–721.
- Janjic, Z.I., 2003. A nonhydrostatic model based on a new approach. *Meteorol. Atmos. Phys.* 82, 271–285.
- Jiang, S.H., Ren, L.L., Hong, Y., Yong, B., Yang, X.L., Yuan, F., Ma, M.W., 2012. Comprehensive evaluation of multi-satellite precipitation products with a dense rain gauge network and optimally merging their simulated hydrological flows using the Bayesian model averaging method. *J. Hydrol.* 452, 213–225.
- Johnson, J.T., MacKeen, P.L., Witt, A., Mitchell, E.D., Stumpf, G.J., Eilts, M.D., Thomas, K.W., 1998. The storm cell identification and tracking algorithm: an enhanced WSR-88D algorithm. *Weather Forecast.* 13, 263–276.
- Kober, C., Craig, G.C., Keil, C., Dornbrack, A., 2012. Blending a probabilistic nowcasting method with a high-resolution numerical weather prediction ensemble for convective precipitation forecasts. *Q. J. R. Meteorol. Soc.* 138, 755–768.

- Li, L., Schmid, W., Joss, J., 1995. Nowcasting of motion and growth of precipitation with radar over a complex orography. *J. Appl. Meteorol.* 34, 1286–1300.
- Lin, Y.L., Farley, R.D., Orville, H.D., 1983. Bulk parameterization of the snow field in a cloud model. *J. Clim. Appl. Meteorol.* 22, 1065–1092.
- Lin, C., Vasic, S., Ki Lambi, A., Turner, B., Zawadzki, I., 2005. Precipitation forecasting skill of numerical weather prediction models and radar nowcasts. *Geophys. Res. Lett.* 32, L14801. <http://dx.doi.org/10.1029/2005GL023451>.
- Macpherson, B., 2001. Operational experience with assimilation of rainfall data in the Met Office Mesoscale model. *Meteorol. Atmos. Phys.* 76, 3–8.
- Mueller, C., Saxen, T., Roberts, R., Wilson, J., Betancourt, T., Dettling, S., Oien, N., Yee, J., 2003. NCAR Auto-Nowcast System. *Weather Forecast.* 18, 545–561.
- Pierce, C.E., Collier, C.G., Hardaker, P.J., Haggett, C.M., 2000. GANDOLF: a system for generating automated nowcasts of convective precipitation. *Meteorol. Appl.* 8, 341–360.
- Raftery, A.E., Gneiting, T., Balabdaoui, F., Polakowski, M., 2005. Using Bayesian model averaging to calibrate forecast ensembles. *Mon. Weather Rev.* 133, 1155–1174.
- Reich, S., 2007. An explicit and conservative remapping strategy for semi-Lagrangian advection. *Atmos. Sci. Lett.* 8, 58–63.
- Rinehart, R., Garvey, E., 1978. Three-dimensional storm motion detection by conventional weather radar. *Nature* 273, 287–289.
- Seed, A.W., 2003. A dynamic and spatial scaling approach to advection forecasting. *J. Appl. Meteorol.* 42, 381–388.
- Shoji, T., Kitaura, H., 2006. Statistical and geostatistical analysis of rainfall in central Japan. *Comput. Geosci.* 32, 1007–1024.
- Sloughter, J.M., Raftery, A.E., Gneiting, T., Fraley, C., 2007. Probabilistic quantitative precipitation forecasting using Bayesian model averaging. *Mon. Weather Rev.* 135, 3209–3220.
- Smith, P.L., Myers, C.G., Orville, H.D., 1975. Radar reflectivity factor calculations in numerical cloud models using bulk parameterization of precipitation. *J. Appl. Meteorol.* 14, 1156–1165.
- Sokol, Z., 2007. Utilization of radar reflectivity for a very short range precipitation forecast. *Czech Meteorol. Bull.* 60, 136–146.
- Sokol, Z., 2011. Assimilation of extrapolated radar reflectivity into a NWP model and its impact on a precipitation forecast at high resolution. *J. Atmos. Res.* 100, 201–212.
- Sokol, Z., Pesice, P., 2012. Nowcasting of precipitation–advection statistical forecast model (SAM) for the Czech Republic. *J. Atmos. Res.* 103, 70–79.
- Sokol, Z., Kitzmiller, D., Pesice, P., Mejsnar, J., 2013. Comparison of precipitation nowcasting by extrapolation and statistical-advection methods. *J. Atmos. Res.* 123, 17–30.
- Sun, W.Y., Chang, C.Z., 1986. Diffusion model for a convective layer. Part I: numerical simulation of convective boundary layer. *J. Clim. Appl. Meteorol.* 25, 1445–1453.
- Tong, M., Xue, M., 2005. Ensemble Kalman filter assimilation of Doppler radar data with a compressible nonhydrostatic model: OSS experiments. *Mon. Weather Rev.* 133, 1789–1807.
- Turner, B., Zawadzki, I., Germann, U., 2004. Predictability of precipitation from continental radar images. Part III: Operational Nowcasting Implementation (MAPLE). *J. Appl. Meteorol.* 43, 231–248.
- Vila, D.A., Machado, L.A.T., Laurent, H., Velasco, I., 2008. Forecast and Tracking the Evolution of Cloud Clusters (ForTraCC) using satellite infrared imagery: methodology and validation. *Weather Forecast.* 23, 233–245.
- Wang, G.L., Wong, W.K., Liu, L.P., Wang, H.Y., 2013. Application of multi-scale tracking radar echoes scheme in quantitative precipitation nowcasting. *Adv. Atmos. Sci.* 30 (2), 448–460.
- Wang, G.L., Hong, Y., Liu, L.P., Wong, W.K., Zahraei, A., Lakshmanan, V., 2014. Intercomparison of quantitative radar-derived precipitation nowcasting schemes in Jianghuai River Basin, China. *Meteorol. Appl.* <http://dx.doi.org/10.1002/met.1451>.
- Weygandt, S.S., Shapiro, A., Droegemeier, K.K., 2002. Retrieval of model initial fields from single-Doppler observations of a supercell thunderstorm. Part I: Single-Doppler velocity retrieval. *Mon. Weather Rev.* 130, 433–453.
- Wilson, J., Xu, M., 2006. Experiments in blending radar echo extrapolation and NWP for nowcasting convective storms. Proceedings, Fourth European Conference on Radar in Meteorology and Hydrology, Barcelona, Spain, pp. 519–522.
- Wolfson, M.M., Dupree, W.J., Rasmussen, R., Steiner, M., Benjamin, S., Weygandt, S., 2008. Consolidated Storm Prediction for Aviation (CoSPA). American Meteorology Society 13th Conference on Aviation, Range, and Aerospace Meteorology, New Orleans, LA.
- Wong, R.K.W., 1977. Weibull distribution, iterative likelihood techniques and hydrometeorological data. *J. Appl. Meteorol.* 16, 1360–1363.
- Wong, W.K., Lai, E.S.T., 2006. RAPIDS – operational blending of Nowcast and NWP QPF. 2nd International Symposium on Quantitative Precipitation Forecasting and Hydrology, Boulder, USA, 4–8 June 2006.
- Wong, W.K., Yeung, L., Wang, Y.C., Chen, M.X., 2009. Towards the blending of NWP with nowcast: operation experience in B08FDP. World Weather Research Program Symposium on Nowcasting, Whistler, BC, Canada, 30 Aug–4 Sep 2009.
- Xie, P.P., Xiong, A.Y., 2011. A conceptual model for constructing high-resolution gauge-satellite merged precipitation analyses. *J. Geophys. Res.* 116, D21106. <http://dx.doi.org/10.1029/2011JD016118>.
- Xue, M., Droegemeier, K.K., Wong, V., 2000. The Advanced Regional Prediction System (ARPS) – a multiscale nonhydrostatic atmospheric simulation and prediction tool. Part I: model dynamics and verification. *Meteorol. Atmos. Phys.* 75, 161–193.
- Xue, M., Droegemeier, K.K., Wong, V., Shapiro, A., Brewster, K., Carr, F., Weber, D., Liu, Y., Wang, D.H., 2001. The Advanced Regional Prediction System (ARPS) – a multiscale nonhydrostatic atmospheric simulation and prediction tool. Part II: model physics and applications. *Meteorol. Atmos. Phys.* 76, 143–165.
- Xue, M., Wang, D.H., Gao, J.D., Brewster, K., Droegemeier, K.K., 2003. The Advanced Regional Prediction System (ARPS), storm-scale numerical weather prediction and data assimilation. *Meteorol. Atmos. Phys.* 82, 139–170.
- Yang, D.D., Shen, S.H., Shao, L.L., Zou, L.J., 2010. A study on blending radar and numerical weather prediction model products. *Meteorol. Mon.* 36 (8), 53–60 (in Chinese).
- Zahraei, A., Hsu, K., Sorooshian, S., Gourley, J.J., Lakshmanan, V., Hong, Y., Bellerby, T., 2012. Quantitative precipitation nowcasting, a Lagrangian pixel-based approach. *J. Atmos. Res.* 118, 418–434.
- Zahraei, A., Hsu, K., Sorooshian, S., Gourley, J.J., Hong, Y., Behrangi, A., 2013. Short-term quantitative precipitation forecasting using an object-based approach. *J. Hydrol.* 483, 1–15.
- Zalesak, S.T., 1979. Fully multidimensional flux-corrected transport algorithms for fluids. *J. Comput. Phys.* 31, 335–362.
- Zhang, X.Z., 1996. Parameter estimate method application of Weibull distribution. *Acta Meteorol. Sin.* 54, 108–116 (in Chinese).
- Zhang, J., Howard, K., Gourley, J.J., 2005. Constructing three dimensional multiple-radar reflectivity mosaics: examples of convective storms and stratiform rain echoes. *J. Atmos. Ocean. Technol.* 22, 30–42.